Signal-in-space Measurements using Microcopters

19th International Flight Inspection Symposium (IFIS) 2016, Belgrade, Serbia

Jochen Bredemeyer
FCS Flight Calibration Services GmbH
Braunschweig, Germany
E-mail: brd@flightcalibration.de

Thorsten Schrader
Physikalisch-Technische Bundesanstalt (PTB)
Braunschweig, Germany
E-mail: Thorsten.Schrader@ptb.de

ABSTRACT

An unmanned aerial system (UAS)-based measurement process to supplement conventional flight inspection of terrestrial navigation aids is described. In contrast to typical flight inspection with an aircraft, the platform allows quasi-stationary hovering in critical areas with extended observation times, without using expensive manned helicopters to carry measurement equipment and antennas.

A microcopter carries the payload which consists of a short linear antenna and a highly miniaturized, FPGA-based large bandwidth receiving/recording system. In contrast to conventional methods, the raw band pass signal-in-space covering the complete channel bandwidth is sampled at a high data rate, and is directly recorded without any pre-processing whatsoever. This preserves maximum opportunities for any signal post-processing to extract all essential parameters of interest. Among typical flight guidance parameters such as DDM, the nature of scatterers can be shown in the time and frequency domains. All data is synchronized in time with the flight vector gained from an advanced on-board position system.

The paper describes experiences gained with the system, and provides first measurement results obtained from ILS localizer and VOR facilities.

INTRODUCTION

Absolute field strength and signal-in-space (SIS) measurements have been performed by using manned helicopters, aircraft or ground vehicles with extendable masts where necessary. Also helium-filled balloons and blimps have been used in the past. Drawbacks of their operation are high costs, fast movement (no repetitive measurement samples can be taken at the same spot), limited maneuverability, long setup time, or, in case of a mast, limited air space to be covered. Now, with the availability of unmanned aerial systems (UAS) such as microcopters a versatile and comparatively cost-effective platform can be deployed for such purposes. Fields of application such as aerial photography, infrared spectroscopy and thermometry, surveillance, inspection and service, surveying, etc. are partly already firmly established with many small companies offering these services. However, these platforms also offer several features that drastically improve the effectiveness of SIS measurements. Here, the UAS is used for precision electromagnetic field and signal measurements of CNS facilities defined in ICAO Annex 10 [1]. This is a task which cannot be assessed sufficiently by conventional flight inspection (FI), and is beyond of the procedures defined in DOC8071 [2].

In the current WERAN project (German abbreviation for “Measuring the potential interaction of wind turbines with terrestrial navigation and radar systems” – [3] – supported by

the Federal Ministry of Economic Affairs and Energy on the basis of a decision by the German Bundestag [grant: 0325644A]), the potential interaction between wind turbines and terrestrial navigation / radar systems is investigated. The frequencies of interest span across the rather wide frequency range of 200kHz to 5GHz. The measurements presented in this paper were performed employing the measurement platform developed in the WERAN project.

DESIGN OF A MEASUREMENT SYSTEM

Among the numerous design requirements for the microcopter (here: octocopter) designated "PTBee" (cp. Fig. 1, 2) a few stand out:

- smooth pre-planned and highly precise operation, also in adverse (e.g. windy) weather conditions
- Electromagnetic Compatibility (EMC) issues
- necessity to calibrate the receiving antenna factor
- various electrical requirements
- quick exchange of batteries

Electromagnetic Compatibility (EMC) issues were of particular importance. On the one hand, motor speed controller switching and high motor lead and battery currents have the potential to cause internal EMC problems such as affecting the magnetic sensor controlling the yaw angle, but also to cause interference with the fields to be measured, especially at frequencies up to a few hundred MHz. On the other hand, it is intended to fly in electromagnetically saturated environments, e.g. at airports or in the vicinity of a radar. Therefore, shielding against high power RF external sources is a basic requirement to protect the UAS itself. This shielding will also reduce inherent emissions from the UAS. Since payload weight and dimension is limited on all flying platforms, the shielding has to be of light weight. To reach the defined safety limits, all electronic instrumentation need to be encapsulated by the shielding, including motor controllers, flight and navigation controllers, data sampling/storage unit and batteries. To prevent overheating of the now internal electronics, a mesh shielding was designed that allows for some air flow. Another advantage of the mesh shielding is that the internal barometric pressure sensor of the UAS contributing to the height information relative to the ground level is not affected.

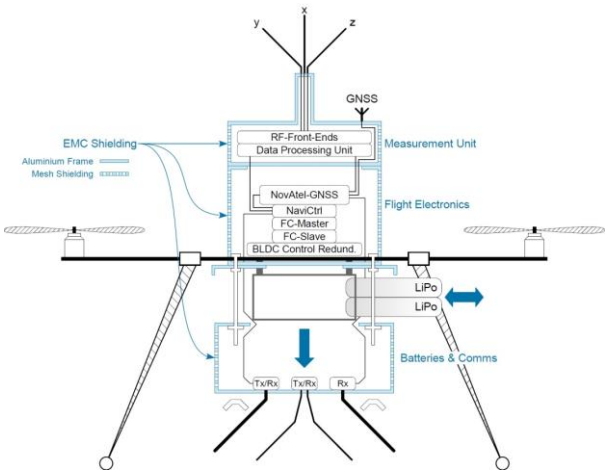

Fig. 1: Mechanical setup of the UAS with the battery tray opened

A low-weight aluminum frame with top and bottom plates and with mesh inserts forms the outer body of the shielding that takes all of these conditions into account. The top plate also serves as mounting pad for the different sensing heads and the GNSS antenna. The inner part of the bottom plate can be unlocked and released, thereby providing access to the battery compartment. A quick exchange feature was designed for the shielded battery. The outer ring of the lower plate serves as support for the antenna of the remote-control receiver, the downlink for the flight status to be received by a smartphone application, and the uplink for a potential differential navigation correction signal. All input and output signal paths are filtered using narrowband band pass filters.

Fig. 2: Photograph of electromagnetically shielded octocopter.

PRECISION NAVIGATION USING RTK

The navigation capabilities include a state-of-the-art NovAtel OEM615 global navigation satellite receiver [4] (GNSS: GPS+EGNOS, GLONASS) and ground differential correction transmitter to enable precise localisation of the UAS. Platform stability is granted by hybridization of GNSS with

motion and rotation sensors of an inertial navigation system (INS). This forms a real-time kinematic (RTK) capability at a sensor update-rate of 20Hz that controls the eight rotors.

A major advantage of such UAS is their ability to approach predefined waypoints (WP) (cp. Fig. 3), a point in space (WGS84 format horizontally and height above ground), and to trigger some action when the WP has been reached. A software tool [5] uses geo-referenced satellite images as maps to define the WPs. Once defined, the WP data is transmitted to the UAS with all necessary parameters such as horizontal and vertical (ascending/descending) speed, waypoint radius (WPR), dwell time at the waypoint, steering of the UAS towards a fixed cardinal direction or towards one or a set of predefined points of interest (POI). After the automatic start procedure, the microcopter moves to the first WP. The predefined WPR between 1 m and 10 m determines the region in space around a WP, where the navigation controller assumes that the given waypoint has been reached.

Fig. 3: Flight track with waypoints (WP) and point of interest (POI)

During its operation the UAS transmits the current position of the UAS including the altitude above ground, the time stamp, and the validity of the measurement data using another radio link. This flight log data can be displayed in real-time on an Android-based smartphone, for which an application has been written.

SIGNAL RECEPTION AND PROCESSING

RF front-ends and antennas

A variety of linear antennas has already been developed for different frequencies and applications. For simplicity, the radiation pattern of each antenna should be as close as possible to an ideal, electrical short, linear antenna [7]. Since the radiation pattern is not ideal, a model for real antennas has been developed. The signal of the real antenna is modelled as a superposition of the signals of an ideal isotropic and an ideal linear antenna. The parameters for this model are again determined through calibration in a known electrical field.

At a later stage it is intended to measure the field strength of three probes where each probe is sensitive for one field component in an orthogonal system. Hence, the data processing unit is capable to sample up to three received signals at full coherence. This allows to calculate the electrical field vector. Consequently, scalar or two-dimensional measurements are also possible.

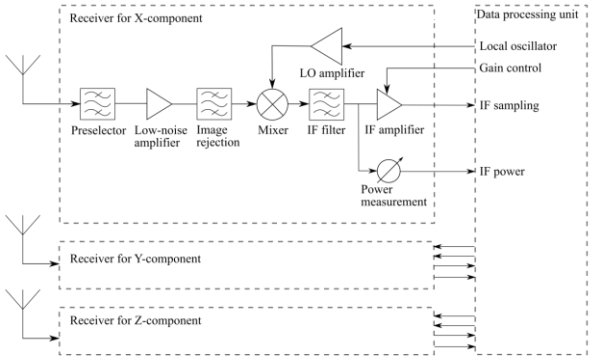

Fig. 4: Block diagram of the RF frontend.

For the various CNS radio bands different RF frontends can be connected to the data processing unit in a modular fashion using the same electrical and mechanical interface (Figure 4).

Signal processing

The RF signal is amplified, filtered and down-converted to an intermediate frequency (IF) using a local oscillator (LO) signal from the data processing unit. The IF signal is then filtered by a Surface-Acoustic-Wave (SAW) filter to suppress undesired mixing products and adjacent RF channels. The IF signal is sampled and stored by the data processing unit using a fast analog-to-digital converter (ADC) and a solid-state disc (SSD) as mass storage device. All further signal analysis that is required to demodulate the signal's content is performed in post-processing using software-define radio (SDR) algorithms after the data has been copied from the SSD. Working on the raw band pass samples allows a maximum of flexibility to derive the relevant information from the signal-in-space. This post-processing is performed through specific algorithms implemented in the C++ language.

An embedded processor hosted on a FPGA-based design manages the data streams from various sources. Fully time-synchronized position information is obtained from the RTK and recorded as well.

To ensure a high dynamic range a digital automatic gain control (AGC) drives variable gain amplifiers (VGA) in the IF section. Highly integrated amplifiers are used for the receiver providing sufficient overall gain, low noise figure, and high bandwidth. The entire system is fully phase-coherent: A single, stable crystal oscillator drives all frequency-dependant components such as ADC clock and LOs.

Undersampling technique

According to the Nyquist criterion the sampling frequency needs to be twice the signal bandwidth to prevent aliasing:

$$f_S > 2\Delta f \qquad (1)$$

Undersampling corresponds with the use of a sampling frequency which is less than the highest frequency present in the signal. In Figure 5 (taken from [5]) this principle is illustrated in the frequency domain. Signals below $0.5f_S$ are located in the so-called first Nyquist Zone (NZ), see (A). Sampling these signals preserves their original carrier frequency. The number of NZ increments by every $0.5f_S$. Frequencies higher than half the sampling rate are folded back into the 1st NZ. Hence, a signal located in any higher NZ will give an image in the first NZ (B, C). No signal information is lost except for the value of the original carrier frequency f_C. An additional frequency reversal occurs if signals are located in even Nyquist zones (B).

If equation

$$f_S = \frac{4f_C}{2NZ-1} \qquad (2)$$

Applies, then the image of f_C is safely placed in the center of the first NZ (= $0.25\ f_S$) [6].

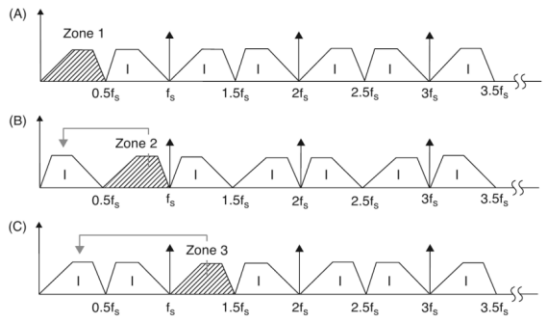

Figure 5: Nyquist zones and frequency translation [6]

The primary function of an anti-aliasing filter is to ensure that the band of sampled signals must not overlap any multiple of $f_S/2$, i.e. it is limited to a unique Nyquist zone. For this purpose, a steep SAW band pass filter is placed in the receiver's IF section. The ILS LOC/VOR RF frontend offers a 70MHz IF. After further amplification on the digitizer board, this signal is then initially sampled at 95MHz. This converts the IF into the second NZ, resulting in an image in first NZ at 25 MHz. A chain of FIR (Finite Impulse Response) decimation band pass filters inside the FPGA then reduces the sampling rate dramatically by the factor of 54, but finally it remains well above twice the channel bandwidth of VHF navigation facilities (<25 kHz) when stored on the SSD.

FLIGHT TESTS AND RESULTS

First tests were performed to receive VHF RF channels using a single horizontally polarized short dipole as shown in Figure 9.

ILS LOC

At Braunschweig airport (EDVE) trials to receive the ILS 2F-localizer were performed. These flights took place while hovering above the threshold of runway 26. Since the raw band pass signal is recorded, the specific signal contents of course and clearance components can be shown separately. As an example, the LOC frequency spectrum at high resolution at a specific point in flight time for both signal components is shown in Figure 6. A sliding window over the band pass signal defines the number of ADC samples that feed a Short-Time Discrete Fourier Transformation (STDFT) that visualizes the spectrum.

On centerline the CRS signal is significantly stronger than CLR (ratio >20dB, height dependant), therefore signal-to-noise ratio of CRS is also higher which can be read from the curves.

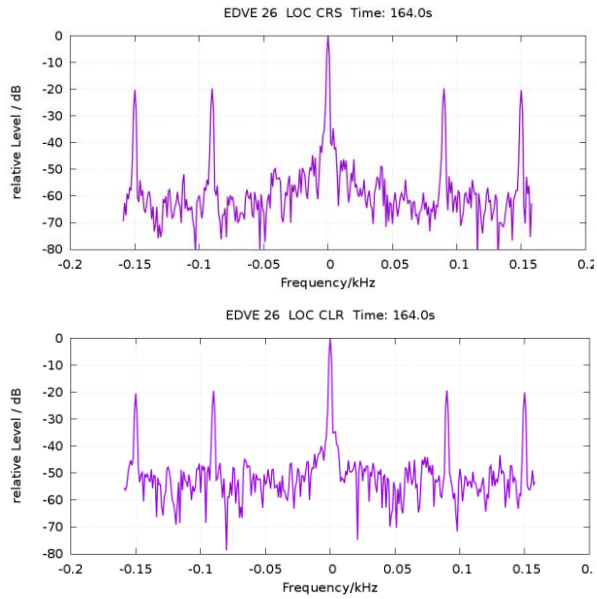

Figure 6: Spectrum of Localizer Course and Clearance gained from band pass signal

In the time domain, the DDM can be derived from the band pass signal by simply demodulating the 90Hz and 150Hz tones using appropriate SDR algorithms.

During a hovering maneuver perpendicular to the centerline at threshold 26 the computed DDM of the right half sector (mod. 150Hz > mod. 90Hz) is given by Figure 7. The left Y-axis gives the displacement angle of the microcopter position against centerline (purple curve), whereas the right Y-axis depicts the DDM.

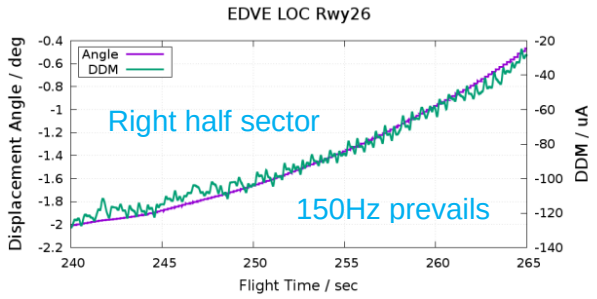

Figure 7: Unfiltered raw DDM of right half sector during hovering flight at THR perpendicular to centerline

A non-linear increase of the raw unfiltered DDM (green) curve can be observed since the flight path was perpendicular to the centerline and not a part of an orbit.

Doppler VOR

Using the data gained from microcopter flights, also radiations from VOR facilities can be assessed showing a large amount of details that conventional flight inspection cannot provide.

In case of a Doppler VOR, it is now possible to fully separate the signals from the center antenna (30Hz AM reference) and the sideband antennas (SBO, 30Hz FM azimuth dependant).

The SBO signal will be analyzed by measuring the frequency deviation of the 9960Hz carriers. As well known, a full 360° turn of the SBO gives one period of a 30Hz oscillation. In Figure 8 the X-axis of the diagram has 50 time slots which corresponds to current DVOR facilities in Germany that have 50 sideband antennas. Within these time slots, the application of the STDFT results in the FM frequency deviation up to 480Hz (left Y-axis) and the amplitude (right Y-axis). Actually, Figure 8 shows a reference curve with a synthesized VOR signal in a lab, which is done for calibration purposes. The 30Hz tone curve deviates from a perfect sine since the number of samples per time slot and therefore the resolution of the STDFT is limited (here: ~1200). Over the period, the amplitude reveals some variances within 0.5dB. This is also due to the resolution limitations across the very short slot observation time of 1/(30*50)sec = 0.67msec .

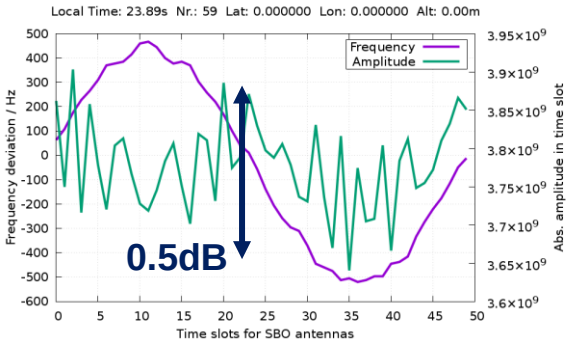

Figure 8: VOR 30Hz SBO frequency deviation in 50 time slots

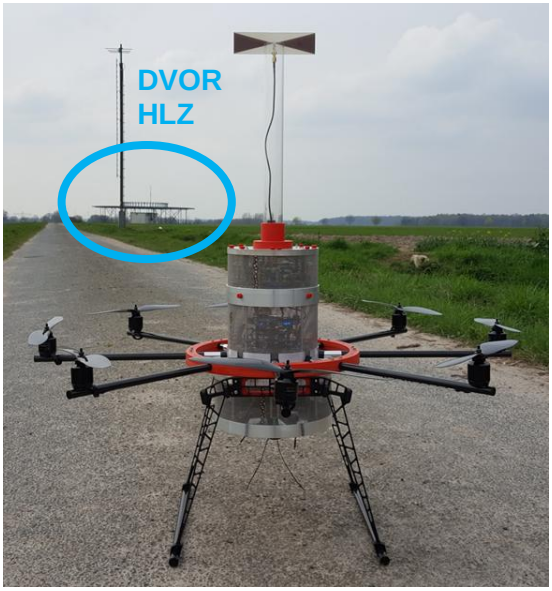

Figure 9: Reference measurement on ground close to DVOR HLZ

Next, a real signal-in-space of 'DVOR Hehlingen' (HLZ) was recorded on the ground close to the transmitter as shown in Figure 9.

During a 30Hz period, the SBO radiation takes place from the different antenna positions above the counterpoise. A significant variation of the field strength over one full rotation is expected. This behavior is shown in Figure 10: The signal strength varies over roughly 6dB and reveals two significant maxima and minima. In fact, the diagram shows an overlay of the Lower sideband and the Upper sideband antenna. So there are always two opposite antennas which have nearly the same radiation characteristics from the receiver's point of view.

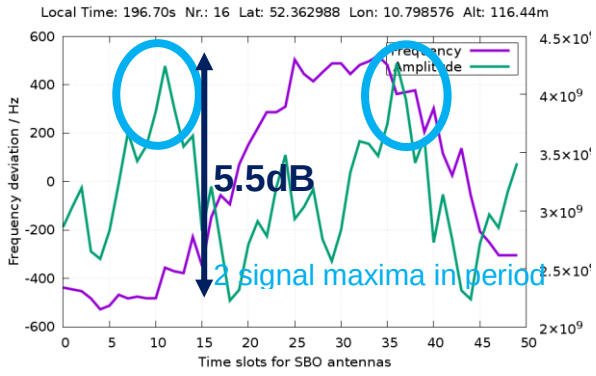

Figure 10: Characteristic Doppler shift and level of DVOR SBO antennas on ground

Even more interesting is the course of the 30Hz tone derived from the frequency deviations. A significant distortion becomes apparent in this unfiltered view (purple curve). The time slots are not synchronized to the antenna numbers, and within one time slot not a single SBO antenna but a mixture of two of them is active due to the SBO blending modulation. But it can be clearly observed that the increase and the decrease of the frequency deviation within 480Hz does not consist of monotone steps. From one slot to another, instead alternating step-ups and step-downs are present in the unfiltered curve. Applied to numerous succeeding pictures of the 30Hz Doppler rotations, comparable to a motion picture, these diagrams always show the same characteristics.

However, in a navigation receiver the 30Hz tone that must be precise in phase will be reconstructed by band pass filtering to ensure the well-known DVOR performance.

These VOR measurements in the lab and on ground provide an overview of the expected performance, before some more degrees of freedom are introduced by the hovering octocopter platform. These measurements were subsequently carried out in the surrounding of DVOR HLZ. In Figure 11 the received center antenna signal level (purple, left Y-axis) and the flight altitude (WGS83, right Y-axis) over flight time at a specific point (constant radial) is shown during the octocopter ascent. At 120sec, a significant level variation becomes visible. These notches are due to the vertical pattern of the DVOR center antenna over the counterpoise and terrain. An example of the already introduced switching behavior of the SBO antennas at free line-of-sight to the DVOR is given by Figure 12. Frequency and amplitude curves show similar characteristics as already seen on the ground (cp. Fig. 10).

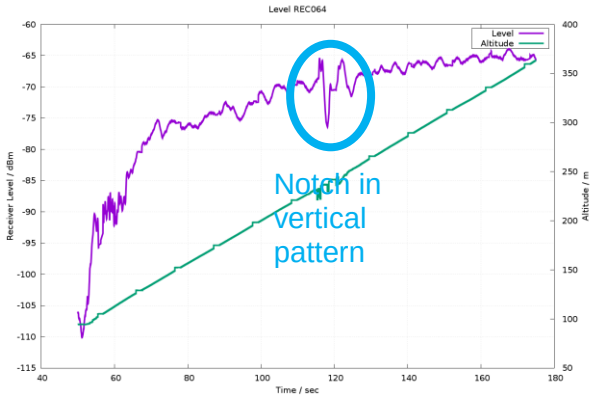

Figure 11: DVOR signal level of vertical octocopter flight

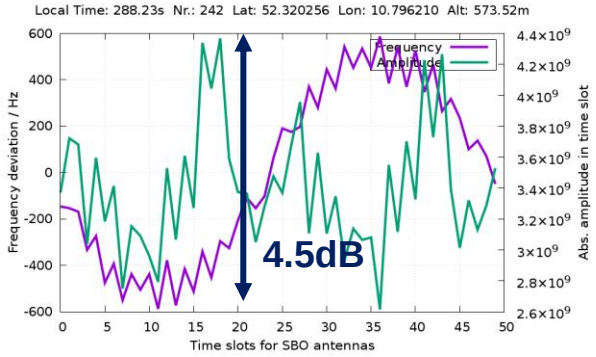

Figure 12: SBO switching as signal-in-space during octocopter flight

Moving the octocopter to a position where the Fresnel zone of free space radiation is affected by a rough edge (forest), some anomalies occur in the signal-in-space as shown by the frequency deviation diagrams: In Figure 13 the Doppler frequency steps (purple) vary much more from the known course in free space or on ground. Especially in slot 25, a strong positive frequency step (marked) to +250Hz occurs. Simultaneously, there is a significant decline in signal amplitude, so that the overall dynamic increases to 8.5dB, compared to 4.5dB in Figure 12.

As more of these anomalies occur in numerous succeeding 30Hz Doppler rotations, the more the phase is affected and slightly shifted. This will eventually contribute to a bearing error as experienced by an aircraft using the DVOR for navigation.

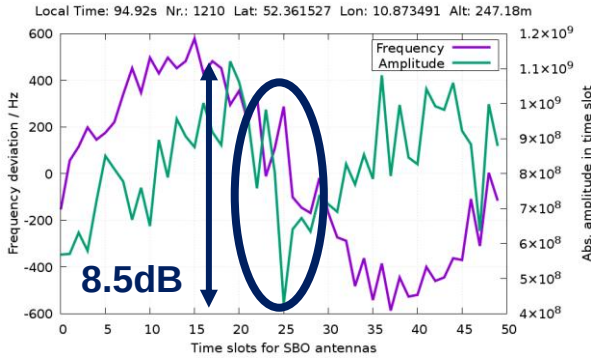

Figure 13: Anomalous SBO switching received in some slots due to multipath propagation

All in all, this shows the complexity and the differences in radiation of the single SBO antennas of a Doppler VOR.

It is the purpose of this new measurement equipment to reveal these signal-in-space anomalies which in turn will for example allow to precisely locate the nature of the source of a Navaid's signal degradation.

GBAS

As the receiver is suitable for VHF navigation band, a useful application may also be the measurement of the GBAS signal-in-space. Just for testing purposes, the transmitter at Braunschweig airport (117.95MHz) was recorded as a band pass signal. Using the STDFT, a spectrum of the signal around the center frequency was computed that is shown in Figure 14. Since the GBAS transmission is time-slotted (16 slots/sec) and the observation time for the spectrum was 1sec, the result for one specific slot may vary. Existing data can be used to synchronize the beginning of a time slot with demodulated D8PSK contents, but this was not done for this paper. Future application may derive the absolute field strength and the bit error rate at specific positions in air space.

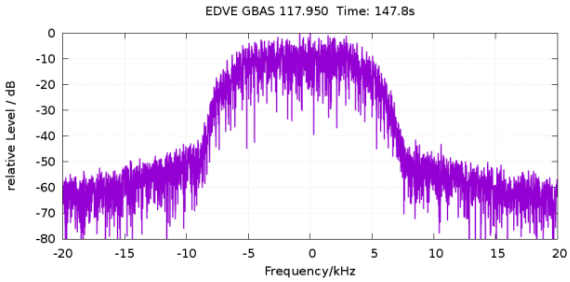

Figure 14: IF spectrum of GBAS during octocopter flight

CONCLUSIONS

A new method based on a UAS octocopter platform was introduced to measure the signal-in-space of Navaids and GBAS. The successful, technologically highly challenging design and integration a small commercially available UAS with an FPGA based high bandwidth multi-channel recording system, calibrated antennas, high-performance receivers and the design elements necessary to operate the octocopter in the vicinity of wind turbines and NAV or radar systems provides a so far unknown high level of insight into RF signal behavior and propagation-related interaction with the topographic context of the ground installation. Due to their small size and hovering capability such systems are well suited to supplement conventional flight inspection. Especially where prolongued observation times of the SIS are required and/or conventional aircraft are unable to reach the measurement positions of interest, the UAS described will allow to obtain the relevant data.

The precision flight paths along predefined waypoints were provided by a real-time kinematic localization system with 20 Hz update rate. The experience so far is that even in heavy wind conditions the octocopter was stable and safe to operate.

The system still has a preliminary design status and further flight tests and design work will be required to achieve all initial design requirements and to fully explore the potential of this new and exciting technology.

UPCOMING WORK

Implementing full three-channel usage will further extend the capabilities to obtain a 3D field vector representation of the measured signals.

A process will be developed to calibrate the overall platform and its antenna factors to SI units, thus allowing a transition from (relative) receiver levels to absolute field strength values.

Further validation measurements using reference dipoles on the open area test site of PTB will improve the confidence in the overall results and the specified operational measurement uncertainty, in compliance with the introduction and usage of specified uncertainties according to [8].

REFERENCES

[1] ICAO Annex 10, Volume I, Radio Navigation Aids, Sixth Edition, July 2006

[2] ICAO DOC 8071, Volume I, Testing of Ground-based Radio Navigation Systems, Fourth Edition – 2000

[3] Schrader T.; Bredemeyer J.; Stupperich C.; Garbe H., "WERAN – Interaction of Wind Turbines with Terrestrial Navigation / Radar Systems," in Electromagnetic Compatibility (EMC), 2015 IEEE International Symposium on, WS14 "Unmanned Aircraft Systems – EMC and Applications," 16-22 Aug. 2015

[4] NovAtel, "Positioning Modes of Operation," Application Note, Rev. 1, 24 Oct. 2013

[5] HiSystems, http://www.mikrokopter.de, 2015

[6] Zumbahlen, H. (Ed.): Linear Circuit Design Handbook, Analog Devices, 2008

[7] Balanis, C.:"Small Dipole" in Antenna Theory, 3rd ed., Hoboken NJ, John Wiley & Sons Inc., 2005.

[8] JCGM 100:2008. Evaluation of measurement data — Guide to the expression of uncertainty in measurement (GUM)